International Journal of Thermal Technologies
E-ISSN 2277 – 4114

Available at http://inpressco.com/category/ijtt/

Research Article

Thermal Analysis of Axial Flux Permanent Magnet Synchronous Motor using 3D Finite Elements

J. Shazly[Á], S. Wahsh[B] and A. Yassin[Á,B*]

[Á]Dept. of Electrical Engineering, Faculty of Engineering, Fayoum University, Fayoum, Egypt
[B]Dept.of Power Electronics and Energy Conversion, Electronics Research Institute, Giza, Egypt

Accepted 06 Dec 2014, Available online 31 Dec2014, **Vol.4, No.4 (Dec 2014)**

Abstract

This paper presents a thermal model of an axial flux permanent magnet synchronous motor (AFPMSM) with the structure of double-stator single-rotor called an axial-flux interior-rotor (AFIR) permanent magnet synchronous machine. The proposed 3D model involves formulation of the heat conduction equations of 3D model using finite element technique. The model considers most of the complexities of the AFPMSM structure to obtain the steady state temperature distribution at any specified location. All significant parameters that influence AFPMSM operation have been taken into consideration. The simulated temperature values are compared with predicted values of previous thermal resistance model and measured one by various authors. In this paper, two different cooling systems are presented and investigated which are natural air and water cooling at different flow rates.

Keywords: *Axial flux permanent magnet synchronous motor (AFPMSM), heat conduction equation, finite-element method, convection.*

1. Introduction

AFPMSM's have various advantages, as they usually are more efficient, since field excitation losses are eliminated. Thus machine efficiency is greatly improved, and higher power density achieved. AFPMSM size and shape are important features in applications where space is limited, so compatibility is crucial. The noise and vibration produced are less than of conventional machines. Also, their air gaps are planar and easily adjustable (Sitapati and Krishnan, 2001). AFPMSM's are used in many different applications nowadays like electrical vehicles, elevators and electric scooters (Acarnly, *et al*, 1996).

The thermal management of the motor is important since the electrical insulation has a temperature limit and affects its efficiency (Fakhfakh, *et al*, 2008). The designers must know the thermal performance of the equipment to choose a suitable cooling strategy.

The rise in the temperature of electric motors under load can cause a problem in many applications (Rosner, 2004). Prior estimation of the thermal behavior becomes a serious matter due to the dependence of the safe operating conditions and overloading capabilities on the temperature rise. The temperature characteristics depend on the winding resistances, consequently the losses and permanent magnet flux. Therefore, the performance analysis of the machine is thermally dependent.

There is lake in literature at analytical and experimental investigations of the temperature distribution of AFPMSM. There are various methods to analyze the thermal behavior of an electrical machine such as finite difference and finite elements (Cannistra and Labini, 1991).Also alternative numerical techniques such as computational fluid dynamics (Staton and So, 1998). The method of "transient thermal circuit" model is used in (Sahin, 2001), which is claimed to give very satisfactory results (Bellenda, *et al*, 1995). Such accuracy and precision can be achieved by the use of finite element method, this method allows the modeling of complicated geometries in 2D and 3D, and gives accurate results without need of many assumptions as the analytical approach does (Sahin, 2001).

This paper describes the mathematical model to investigate the temperature distribution of AFIR using finite element method to solve the 3D heat conduction equations. The numerical simulation of the heat transfer was carried out with a general purpose finite-element based software package, ANSYS for heat transfer problems.

2. Thermal model

The motor handled in this paper has the structure of double-stator single-rotor AFPMSM called AFIR, constructed in slotted stator structure (Platt, 1989), (Parviainenand Pyrhönen, 2004), as illustrated in Fig. 1. AFIR structure, with a rotor located between stators, is simpler, as there is more space for windings (Caricchi, *et al*, 1995), and is preferred in applications which need small inertia because it has very high power-to-inertia ratio (Mahmoud, *et al*, 2011).

*Corresponding author: **A. Yassin**

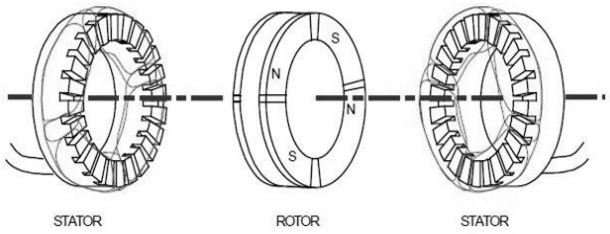

Fig.1AFIR Structure

Fig. 2 and Fig. 3 respectively present the three-dimensional and the side view of an AFIR.

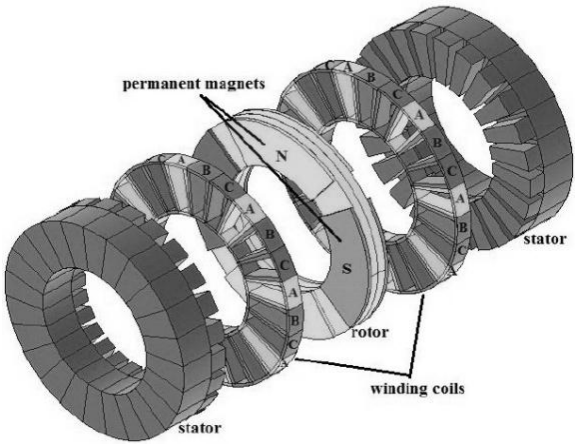

Fig.2 Electromagnetic machine with a disc rotor built by Tesla

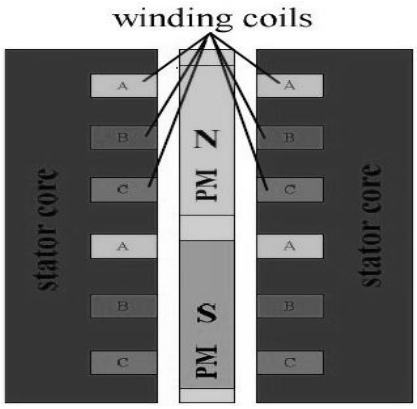

Fig.3 2D side view of slotted stator AFIR

Due to complexity of the 3D model, the theoretical thermal model for AFIR which developed here is limited by the following basic assumptions (Eteiba, *et al*, 2008), (Miller and Hendershot, (1995):

- Due to symmetry, 1/16 of the 3D model is used to simplify the analysis and reduce the simulation time as show in Fig. 4.
- The heat which is generated per unit volume of the iron core is uniformly distributed in it; while that of the copper coils is uniformly distributed in the windings.
- The winding insulation not taken into account as the dielectric loss in winding insulation is assumed to be small compared to copper losses in the conductors and the windings are modeled as solid object.
- The epoxy on the end windings is neglected due to simulation difficulties.
- The thermo-physical properties of cooling fluid, air and AFIR components material are supposed to be temperature dependent.
- Cooling duct is assumed to be divided into two pipes located behind the stator.
- Heat transferred by means of radiation can be mostly neglected as it is generally very small.
- Measured values of ambient temperature are always considered and the initial temperatures of the AFIR components are assumed equal to the ambient temperature.

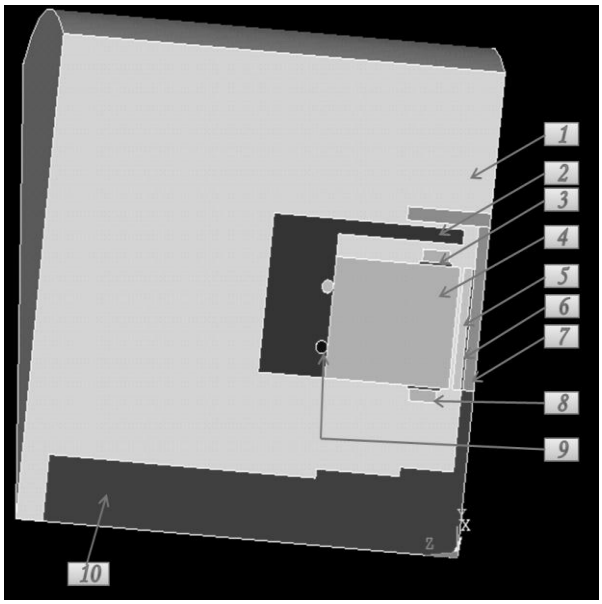

Fig.4 The 3D model of 1/16 of the AFIR (1 air, 2 casing, 3 Pressboard, 4 stator, 5 PM, 6 glue, 7 rotor, 8 copper windings, 9 cooling pipes, 10 shaft)

The AFIR geometrical data and parameters that used in the analysis are summarized in Tables 1 and 2 respectively.
The following differential equation governs the heat conduction for steady state heat transfer of 3-D model (Ozisik, 1985).

$$\frac{d}{dx}\left(K\frac{dT}{dx}\right)+\frac{d}{dy}\left(K\frac{dT}{dy}\right)+\frac{d}{dz}\left(K\frac{dT}{dz}\right)+q^{\circ}=0 \qquad (1)$$

The calculation of losses is essential in terms of an accurate prior estimation of the efficiency and the thermal behavior of the machine. The heat sources inside the AFIR are copper losses, core losses, and mechanical losses. The most significant of these is the copper losses.

The heat generated per unit volume of each component of the machine is:

$$q^{\circ}=\frac{q\ (W)}{volume\ of\ each\ component\ (\mathrm{m}^3)} \qquad (2)$$

Table 1AFIR geometrical data

Machine Parameters	Symbol	Value
Stator outside diameter	D_o	190 mm
Stator inside diameter	D_i	110 mm
Stator yoke length	L_{st}	30 mm
Total stator axial length	L_y	45 mm
Number of poles	$2p$	4
Number of slots/pole/phase	n_{spp}	2
Number of turns/phase/stator	N_{ph}	16
Air gap length	g	1.5 mm
Total (×2) magnet axial length	L_m	6 mm
Slot bottom width	W_{sb}	6 mm
Slot top width	W_s	1.5 mm
Slot depth	d_b	11 mm
Slot top depth 1	d_{t1}	2 mm
Slot top depth 2	d_{t2}	2 mm
Total slot depth	d_s	15 mm

Table 2AFIR parameters

Machine Parameters	Values
Mechanical torque	18 Nm
Maximum speed	16000 rpm
Rated power	30.16 kW
Rated stator current (rms)	53 A
Max. inverter frequency	533 Hz
Line to line emf (rms)	330 V
Terminal voltage	345 V
Phase synchronous inductance,	0.115 mH
Per-unit synchronous reactance	0.203
Air gap flux density, B_{go}	0.735 T

The losses components of the AFIR can be summarized as:

2.1 Copper losses

The copper losses function by phase current (I) and phase resistance (R) (Fakhfakh, *et al*, 2008), and depend on the load as well as the temperature of the windings.

$$q_{coils} = I^2 R \tag{3}$$

2.2 Core losses

Core losses are more significant at higher speeds; they are generally the second largest loss component in AC machines. They can be separated to stator core losses and rotor losses.

2.2.1 Stator iron core losses

The iron losses represent the losses in the stator yoke and teeth (Fakhfakh, *et al*, 2008). The stator core loss density in can be separated into a hysteresis and an eddy current component under alternating flux conditions and can be written in terms of the Steinmetz equation (Miller and Hendershot, (1995) as:

$$P_{fe} = P_h + P_e = c_h \hat{B}^{n(\hat{B})} f + c_e \hat{B}^2 f^2 \tag{4}$$

Where c_h , c_e and n are constants, determined by manufacturer's data.

The Steinmetz equation that describes the specific loss in (W/kg) (Fakhfakh, *et al*, 2008) is:

$$p_{fe} = 0.014492 \hat{B}^{1.9} f + 0.014492 \hat{B}^2 f^2 \tag{5}$$

The iron core loss in watts is determined as:

$$q_{core} = M . p_{fe} \tag{6}$$

Where M is the mass of the iron core in (kg).

2.2.2 Rotor core losses

Rotor losses generated by induced eddy currents may amount to a major part of the total losses in high-speed permanent-magnet machine applications. The eddy currents are mainly induced in the permanent magnets, which are highly conductive, and in the rotor steel too (Van der Veen, *et al*, 1997).

The rotor losses generated by induced eddy currents can be found in the following approximated equation (Cho and Fussell, 1993).

$$q_{rotor} = \frac{\sigma L_m L_i \tau^2 \hat{B}^2 \omega_e^2}{8} \left(\frac{\delta}{3\tau} \frac{\sinh\left(\frac{\delta}{\tau}\right) - \sin\left(\frac{\delta}{\tau}\right)}{\cosh\left(\frac{\delta}{\tau}\right) - \cos\left(\frac{\delta}{\tau}\right)} \right) \tag{7}$$

2.3 Mechanical losses

Friction losses in the air space of high-speed machines greatly contribute to the total losses. Consequently, it is rather important to calculate the friction losses so as to make good estimations of the efficiency and the thermal behavior of the machine (Saari, 1998).The friction torque of a rotating cylinder can be calculated as:

$$T = C_f \rho \Pi \omega^2 r^4 l \tag{8}$$

The friction torque for a rotating disk having inner and outer radii r_i and r_0 respectively can be written as:

$$T = \frac{1}{2} C_f \rho \Pi \omega^2 (r_o^5 - r_i^5) \tag{9}$$

The mechanical loss can be calculated by the following equation:

$$q_{mech} = \omega T \tag{10}$$

All the losses occurring in the AFIR are converted into heat. This heat is transferred to the surrounding air by several stages due to a temperature difference at the boundaries of each stage. Heat is transferred by means of conduction occurring in the solid parts of the machine such as steel, copper and insulation, by convection appearing in the air contained in the machine.

The mathematical formulation of this convection boundary condition is obtained by considering an energy balance at the surface stated as:

$$-K\frac{dT}{dx} - K\frac{dT}{dy} - K\frac{dT}{dz} = h(T - T_B) \tag{11}$$

Some convective heat transfer coefficients must be calculated to determine the temperatures of the present AFIR model. There are convective heat transfer between the windings surface, the stator surface and the air flowing over them, then from the air gap region to the inner surface of the machine, Finally from the external machine frame to the surrounding air.

The convection coefficients are generally the most difficult ones to estimate, although the accuracy and sensitivity of the problem are highly dependent on them. The main problem of the analytical estimation of the convection coefficients is their nonlinear dependency on the temperature. The heat transfer coefficients are also a function of the material properties of the various elements, Specific thermal conductivity, specific density and specific heat capacity values of the selected materials (Sahin, 2001).

The temperature of the permanent magnets depends mainly on the heat transfer between the stator and the rotor in the air-gap region since the permanent magnets are faced directly towards the air-gap. An air-gap heat transfer coefficient with reasonable accuracy is needed. There is an obvious lack of information regarding the thermal modeling of axial-flux machines, since appropriate semi-empirical correlations to define the heat transfer coefficient for the air-gap region of an axial-flux machine are not available (Yliopisto, 2005).

The heat transfer coefficients in the airgap and in the end-air of the machine depend on many factors such as the speed of the flow, temperature, fluid properties, airgap dimensions and even the surface characteristics of the rotating parts. The heat transfer coefficient, between the rotor surface and the air, can be determined by classical Nusselt number (Nu) correlation's as (Sahin, 2001):

$$h = \frac{\mathrm{Nu}.K}{g} \tag{12}$$

The Nusselt number is calculated for the three different regimes (Becker and Kaye, 1962) of Taylor number, based on the measurements conducted by Becker and Kaye, (Saari, 1998), (Becker and Kaye, 1962):

$$Nu = \begin{cases} 2 & for \;\; Ta < 1700 \\ 0.128 Ta^{0.367} & for \;\; 1700 < Ta < 10^4 \\ 0.409 Ta^{0.241} & for \;\; 10^4 < Ta < 10^7 \end{cases} \tag{13}$$

The Taylor number is calculated by using

$$Ta = \frac{RE_g^{\,2}.g}{r} \tag{14}$$

Reynolds number describes the nature of flow, which is the ratio of the inertia and the viscous forces. RE_g is Couette Reynolds number, which describes the tangential flow forced by a rotating rotor with the existence of a stator and a small airgap(Saari, 1998).

$$RE_g = \frac{\nu.g}{g} \tag{15}$$

For the calculation of the heat transfer coefficient between the rotating shaft and the ambient, other known formula can be adopted since the circumferential speed of the small shaft is not as high as that of the outer rotor. It can be written as (Henneberger and Yahia, 1995).

$$h = 15.5(0.3V + 1)\, W/^{o}c\, m^2 \tag{16}$$

It should be pointed out that the convective heat transfer coefficient between the frame and the ambient is based on the assumption that only natural convection is present. Consequently, the corresponding heat transfer coefficient can be taken as a known constant, which is determined in (Henneberger and Yahia, 1995).

$$h = 14\, W/^{o}c\, m^2 \tag{17}$$

The heat transfer coefficient between the frame and the cooling water is similar to the heat transfer in turbulent fluids in tubes (Henneberger and Yahia, 1995). It is defined with the Nusselt number, the specific thermal conductivity of the coolant and the hydraulic diameter as (Henneberger, 1998).

$$h = \frac{\mathrm{Nu}.K}{d_h} \tag{18}$$

The Nusselt number for turbulent fluids in tubes is:

$$\mathrm{Nu} = 0.032\, RE^{0.8}\, \mathrm{Pr}^{0.37}\left(\frac{d_h}{l_h}\right) \tag{19}$$

The Prandtl number describes the relation between the viscosity of the medium at a certain temperature and the thermal conductivity (Binns and Shimmin, 1995). Reynolds number in this case is

$$RE = \frac{\upsilon_w d_h}{g} \tag{20}$$

3. Results and discussion

The Thermal model is verified using finite-element package, ANSYS, and the results (nodal temperatures) are obtained from the thermal analysis. The accuracy of computed results is verified by comparing the predicted results with the measured values and the computed temperature values of previous thermal resistance model.

3.1 Verification of the model

At the case of 6000 RPM, with natural air cooling system, The measured values of the windings, stator and magnet temperatures are recorded in (Sahin, 2001) and also the results of the thermal resistance model at an ambient temperature of 30^{o}C, and with normal air pressure during load I= 42 A, however the actual measured temperature depends on the position of the temperature sensor which is not determined.

When solving the three dimension model using the finite element package, the solution gives the range of temperatures inside the machine. The contour plot for a nodal temperature distribution through windings, stator yoke and magnet, which are resulted from solving using the finite element package, are shown in Fig. 5, Fig. 6 and Fig. 7 respectively. It can be noticed that there is a reasonable agreement between the calculated temperatures and the measured temperature values.

Table 3 shows the comparison between the results of the predicted temperature values of 3D finite element model with the predicted temperature values of previous thermal resistance model, and the measured temperature values.

By comparing the results, it can be found that the 3D finite element model gives temperature distributions for each component and have the advantage of its clarity at each point in the model, where determining the most heated points and the least ones through the model are available.

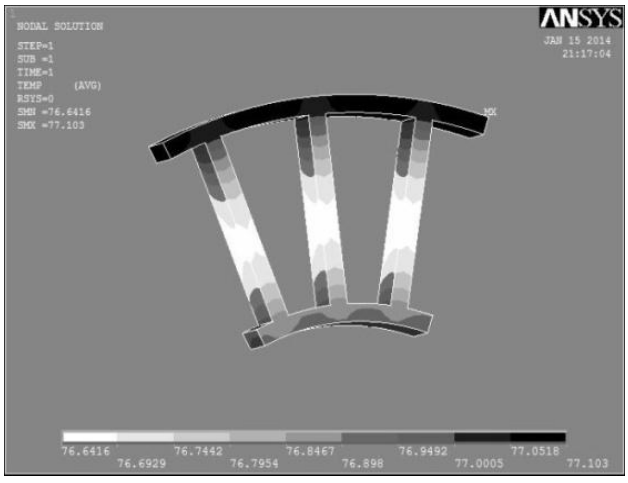

Fig.5 Temperature distribution through the windings

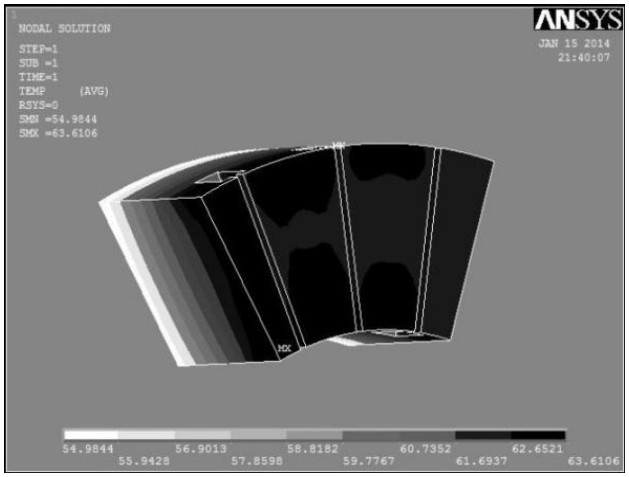

Fig.6 Temperature distribution through the stator yoke

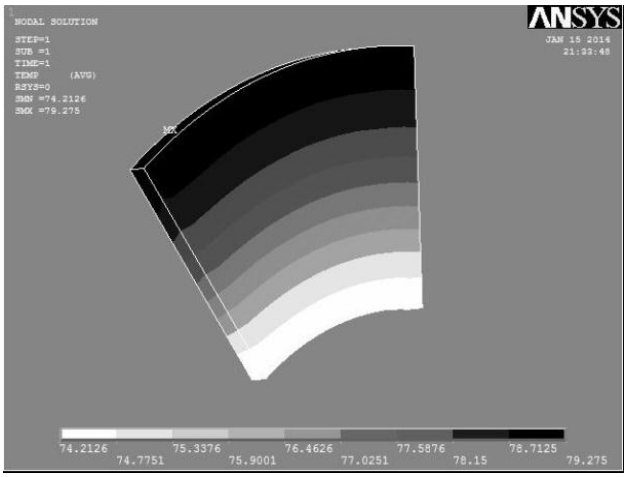

Fig.7 Temperature distribution through the PM

However, the thermal resistance model represents the bulk temperature of each component of the model. The actual measured temperature for each component depends on the position of the temperature sensor. Nevertheless, the position of the measured values is not determined and this makes it not accurate for the overall elements where there are points are more heated than others.

It can also be noticed that the predicted temperature values of the copper windings are lower than the measured values. One possible reason is the assumption which consider that the windings or the coils are modeled as solid objects, where dividing it into cylindrical conductors each covered with insulating varnish makes heat transfer through the windings more difficult thereby the winding temperature increases.

In addition, the end windings of the stator are filled with epoxy (Fakhfakh, *et al*, 2008) and this epoxy on the end windings gives rise to a weak heat transfer from the end windings, causing its temperature value increases. Unfortunately, this epoxy on the end windings is assumed to be neglected, and this may result in slightly low estimated temperature values in the analysis. It can be seen that the most heated points in the copper are at end windings as illustrated in Fig 5.

Table 3 Comparison between the predicted and measured results

Material	Results of 3D FE Model Using ANSYS (℃)			Measurements (℃)	Results of Thermal Resistance model (℃)
	Range		Average		
	Min.	Max.			
Windings	76.64	77.10	76.87	87	83
Stator	54.98	63.61	59.29	54	50.5
Magnet	74.21	79.27	76.74	69	77

Table 4 Predicted temperatures for the 3D model and average temperature of each element at 3L/min and 8L/min of cooling water at an ambient temperature of 30 ^{o}C

Material	Results of 3D FE Model Using ANSYS at 3L/min Rate of Flow of Water Cooling (℃)			Results of 3D FE Model using ANSYS at 8L/min Rate of Flow of Water Cooling (℃)		
	Range		Average	Range		Average
	Min.	Max.		Min.	Max.	
Windings	65.07	65.54	65.30	60.48	60.95	60.71
Stator	42.74	52.18	47.46	37.82	47.65	42.73
Magnet	66.95	71.42	69.18	64.06	68.30	66.18

Table 5 The results of the comparison between calculated average temperatures of the validation case and the cases of 3L/min & 8 L/min water-cooling at 6000 rpm, I = 42 A and an ambient temperature of 30^{o}C

Material	Average Temperature at the Validation Case (℃)	Average Temperature at 3 L/min (℃)	Average Temperature at 8 L/min (℃)
Windings	76.87	65.30	60.71
Stator	59.29	47.46	42.73
Magnet	76.74	69.18	66.18

3.2 Different cooling strategy

The influence of cooling type is very significant at the AFIR components' temperatures because it is one of the most important things that affect the aging rate of the machine.

To reduce the overall temperature of the motor and investigate the influence of changing the cooling strategy on the AFIR components' temperatures, it is suggested to change the cooling strategy by using water in the cooling duct as a cooling fluid instead of the natural air. The analysis was extended to determine the response of AFIR components to changing the flow rate of the cooling water. The analysis was executed when the motor is cooled by water inside cooling pipes located behind the stator at different rates of flow of 3L/min and 8L/min at an ambient temperature of 30 ^{o}C.

Table 4 shows the Results of the predicted temperature values for 3D finite element model using ANSYS and average temperature of each element in the model at 3L/min and 8L/min rates of flow of water cooling at an ambient temperature of 30 ^{o}C.

Table 5 shows a comparison between the average predicted temperature values for 3D Finite Element model using ANSYS of the cases of natural air and (3 L/min, 8 L/min) of water-cooling at 6000 rpm, I = 42 A and an ambient temperature of 30 ^{o}C.

It can be observed that the average temperature of the winding, stator and the magnet reduces when the cooling fluid inside the cooling duct changed to water instead of the natural air. Also it is obviously seen that the average temperatures at rate of flow of 8L/min of water cooling are lower than those at rate of flow of 3L/min of water cooling.

Then, from all the previous cases it can be found that the water cooling is better than cooling by natural air and also the machine's overall temperature is dependent on the flow rate of the cooling fluid since the machine's overall temperature reduces when the flow rate of the cooling fluid increases.

Conclusion

Application of 3D finite-elements to steady state heat conduction equation permits the calculation of the temperatures at any specified location within an AFIR, considering the variations in boundary conditions, and the contributions of the convective heat transfer. When AFIR modeled with natural air cooling system, the analytical approach for evaluating temperature distribution followed in the present investigation seems to correspond adequately well with results of actual measurements.

To reduce the overall temperature of the motor we proposed changing the cooling strategy by using water in the cooling duct as a cooling fluid instead of the natural air at different flow rates of the cooling water of 3L/min and 8L/min.

It was observed that the motor's overall temperature is dependent on the type of the cooling fluid where a wide change in temperatures of the AFIR could be created due to changing the cooling type. And it depends also on the flow rate of the cooling fluid since the machine's overall temperature reduces when the flow rate of the cooling fluid increases. From the results, it is clear that the water cooling is the better solution to cooling the motor under study.

Nomenclature

$\hat{B}$	Amplitude of flux density, T.
C	Specific heat, J/kg.K.
C_f	Friction coefficient, dimensionless.
d_h	Hydraulic diameter, m.
f	Frequency, Hz.
g	Air gap length, m.
h	Convective heat transfer coefficient, W/m2 K.
I	Phase current, A.
K	Thermal conductivity, W/m K.
l	Axial length, m.
l_h	Length of the cooling channel, m.
L_i	Effective length of the stator core in radial direction, m.
L_m	Magnet length, m.
M	Mass of the iron core, kg.
Nu	Nusselt number, dimensionless.
P_{fe}	Stator core loss density, W/kg.
P_h	Hysteresis component, W/kg.
P_e	Eddy current component, W/kg.
Pr	Prandtl number, dimensionless.
q	Loss of each component of the motor, W.
q^o	Heat transfer rate, W/m^3.
q_{coils}	Heat generated in the copper coils of the motor, W.
q_{core}	Heat generated in the iron core of the motor, W.
q_{mech}	Mechanical loss, W.
q_{rotor}	Rotor loss, W.
R	Phase resistance, Ω.
r	Radius of the disk, m.
r_i	Inner radii, m.
r_o	Outer radii, m.
RE	Reynolds number, dimensionless.
RE_g	Couette Reynolds number, dimensionless.
T	Temperature, K.
Ta	Taylor number, dimensionless.
T_B	Bulk temperature, K.
t	Time, s.
V	Velocity of the air, m/s.
x	X direction.
y	Y direction.
z	Z direction.
δ	Skin depth in the magnet for the relevant harmonic frequency.
σ	Stephan-Boltzmann constant.
ρ	Density of the material, kg / m^3.
τ	Pole pitch.
v	Circumferential speed of the rotor m/s.
v_w	Velocity of the water, m/s.
ϑ	Kinematic viscosity of the fluid or gas, m^2/s.
ω	Rotational speed, rpm.
ω_e	Angular frequency of the eddy currents.

References

Acarnly P., Mecrow J., Burdess J.S., Fawchett J.N., Kelly J.G., Dickinson P.G., (1996), Design principles for a flywheel energy store for road vehicles, IEEE Trans. on Industry Applications,vol. 32, pp. 1402-1407.

Becker K.M., Kaye J., (1962), Measurements of diabatic flow in an annulus with an inner rotating cylinder, Trans. of ASME, Journal of Heat Transfer, vol. 84, pp. 97-105.

Bellenda G., Ferraris L., Tenconi A., (1995), A new simplified thermal model for induction motors for EVs applications, IEEE Int. Conf. on Electrical Machines and Drives, pp. 11-15.

Binns K. J., Shimmin D. W., (1995), The Relationship Between Performance Characteristic and Size of Permanent Magnet Motors, IEE Int. Conf. on Electric Machines and. on Drives, 412:423-426.

Cannistra G., Labini M.S., (1991), Thermal analysis in an induction machine using thermal network and finite element method, Fifth International Conference on Electrical Machines and Drives, pp. 300-304.

Caricchi F., Crescimbini F., Santini E., (1995), Basic principle and design criteria of axial-flux PM machines having counter rotating rotors, IEEE Trans. Ind. Appl., vol. 31, pp.1062-1068.

Cho C. P., Fussell B.K., (1993), Eddy current loss calculation in the permanent magnet of a large horse power axial-field motor, Incremental Motion ControlSystems and Devices Proc., pp. 245-254.

Eteiba M. B., Abdel Aziz M. M., Shazly J. H., (2008), Heat conduction problems in SF6 gas cooled-insulated power transformers solved by the finite-element method, IEEE Trans. Power Delivery, vol. 23, pp. 1457 - 1463.

Fakhfakh M. A., Kasem M.H., Tounsi S., Neji R., (2008), Thermal analysis of a permanent magnet synchronous motor for electric vehicles, Journal of Asian Electric Vehicles,vol. 6.

Henneberger G., Yahia K.B., (1995), Calculation and identification of a thermal equivalent circuit of a water cooled induction motor for electric vehicle applications, IEE Int. Conf. on Electrical Machines and Drives, pp. 6-10.

Henneberger S., (1998), Design and Development of a Permanent Magnet Synchronous Motor for a Hybrid Electric Vehicle Drive, PhD thesis.

Mahmoud A., Rahim N. A., Hew W. P., (2011), Axial-flux permanent-magnet machine modeling, design, simulation and analysis, Scientific Research and Essays, vol.6, pp.2525-2549.

Miller T.J.E., Hendershot J.R., (1995), Design of brushless permanent magnet motors, Oxford University Press.

Ozisik M. N., (1985), Heat Transfer a Basic Approach," NewYOrk: McGrawHill.

Parviainen A., Pyrhönen M.N.J., (2004), Design of axial-flux permanent magnet machines: thermal analysis, Proc. Conf. International Conference on Electrical Machines (ICEM), Cracow, Poland.

Platt D., (1989), Permanent magnet synchronous motor with axial flux geometry, IEEE Trans. Magnet, vol.25, pp.3076-3079.

Rosner&Rosner GBR Technical Design Laboratory, (2004), Thermal analysis of electric motors necessity – model – conclusions, ,http://www.rosner-tdl.de/english/ROSNER-TDL_TR-02.pdf.

Saari J., (1998), Thermal analysis of high-speed induction machines, PhD thesis, ActaPolytechnicaScandinavica.

Sahin F., (2001), Design and development of a high-speed axial-flux permanent magnet machine, TechnischeUniversiteit Eindhoven, Proefschrift.-ISBN 90-386-1380-1

Sitapati K., Krishnan R., (2001), Performance comparisons of radial and axial field, permanent-magnet, brushless machines, IEEE Trans. Industr. Appl., vol. 37, pp. 1219-1226.

Staton D.A., So E., (1998), Determination of optimal thermal parameters for brushless permanent magnet motor design, IEEE IAS'98, vol. 1, pp. 41-49.

Van der Veen J.L.F., Offringa L.J.J., Vandenput J.A., (1997), Minimising rotor losses in high-speed high-power permanent-magnet synchronous generators with rectifier load, IEE Proc. Elec. Power Appl., 144(5):331—337.

Yliopisto L.T., (2005), Design of axial-flux permanent-magnet low-speed machines and performance comparison between radial-flux and axial-flux machines, PhD thesis, Lappeenranta university of technology,Lappeenranta, Finland.